Article

Synthesis of MFeS Clusters Containing a Planar M Site (M = Ni, Pd, Pt), a Structural Element in the C-Cluster of Carbon Monoxide Dehydrogenase

Rashmishree Panda, Curtis P. Berlinguette, Yugen Zhang, and Richard H. Holm

J. Am. Chem. Soc., **2005**, 127 (31), 11092-11101• DOI: 10.1021/ja052381s • Publication Date (Web): 13 July 2005

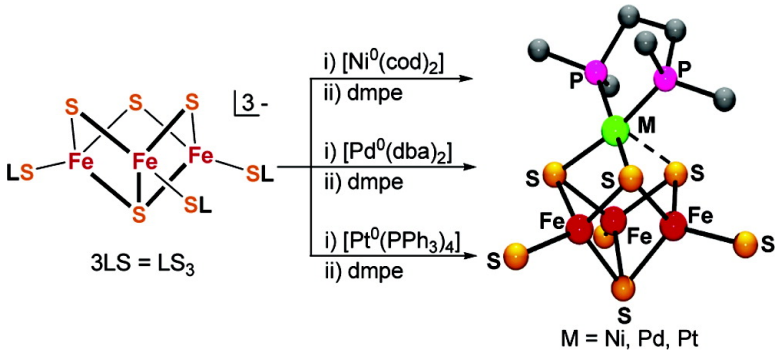

More About This Article

Additional resources and features associated with this article are available within the HTML version:

- Supporting Information
- Links to the 2 articles that cite this article, as of the time of this article download
- Access to high resolution figures
- Links to articles and content related to this article
- Copyright permission to reproduce figures and/or text from this article

View the Full Text HTML

J|A|C|S
ARTICLES
Published on Web 07/13/2005

Synthesis of MFe_3S_4 Clusters Containing a Planar M^{II} Site (M = Ni, Pd, Pt), a Structural Element in the C-Cluster of Carbon Monoxide Dehydrogenase

Rashmishree Panda, Curtis P. Berlinguette, Yugen Zhang, and Richard H. Holm*

Contribution from the Department of Chemistry and Chemical Biology, Harvard University, Cambridge, Massachusetts 02138

Received April 12, 2005; E-mail: holm@chemistry.harvard.edu

Abstract: Synthesis of an analogue of the C-cluster of *C. hydrogenoformans* carbon monoxide dehydrogenase requires formation of a planar Ni^{II} site and attachment of an exo iron atom in the core unit $NiFe_4S_5$. The first objective has been achieved by two reactions: (i) displacement of Ph_3P or Bu^tNC at tetrahedral Ni^{II} sites of cubane-type $[NiFe_3S_4]^+$ clusters with chelating diphosphines, and (ii) metal atom incorporation into a cuboidal $[Fe_3S_4]^0$ cluster with a M^0 reactant in the presence of bis(1,2-dimethylphosphino)ethane (dmpe). The isolated product clusters $[(dmpe)MFe_3S_4(LS_3)]^{2-}$ (M = Ni^{II} (**9**), Pd^{II} (**12**), Pt^{II} (**13**); LS_3 = 1,3,5-tris((4,6-dimethyl-3-mercaptophenyl)thio)-2,4,6-tris(*p*-tolylthio)benzene(3−)) contain the cores $[MFe_3(\mu_2\text{-}S^*)(\mu_3\text{-}S)_3]^+$ having planar $M^{II}P_2S_2$ sites and variable nonbonding M···S* distances of 2.6−3.4 Å. Reaction (i) involves a tetrahedral → planar Ni^{II} structural change between isomeric cubane and cubanoid $[NiFe_3S_4]^+$ cores. Based on the magnetic properties of **12** and earlier considerations, the $S = {}^5/_2$ ground state of the cubanoid cluster arises from the $[Fe_3S_4]^-$ fragment, whereas the $S = {}^3/_2$ ground state of the cubane cluster is a consequence of antiferromagnetic coupling between the spins of Ni^{2+} ($S = 1$) and $[Fe_3S_4]^-$. Other substitution reactions of $[NiFe_3S_4]^+$ clusters and 1:3 site-differentiated $[Fe_4S_4]^{2+}$ clusters are described, as are the structures of **12**, **13**, $[(Me_3P)NiFe_3S_4(LS_3)]^{2-}$, and $[Fe_4S_4(LS_3)L']^{2-}$ (L′ = $Me_2NC_2H_4S^-$, $Ph_2P(O)C_2H_4S^-$). This work significantly expands our initial report of cluster **9** (Panda et al. *J. Am. Chem. Soc.* **2004**, *126*, 6448−6459) and further demonstrates that a planar M^{II} site can be stabilized within a cubanoid $[NiFe_3S_4]^+$ core.

Introduction

All carbon monoxide dehydrogenases catalyze the reaction $CO + H_2O \rightleftharpoons CO_2 + 2H^+ + 2e^-$. Bifunctional enzymes also catalyze the formation of acetylcoenzyme A from carbon monoxide, a methyl group supplied by a corrinoid protein, and coenzyme A.[1−3] The acetylcoenzyme A synthase activity occurs at the A-cluster, a bridged assembly with minimal formulation $[Fe_4S_4]$-$(\mu_2\text{-}S_{Cys})$-$[Ni((\mu_2\text{-}S_{Cys})_2Gly)Ni]$ whose structure has been revealed by protein crystallography[4,5] and dinickel content has been shown to be essential for activity.[5−7] The CO/CO_2 interconversion reaction occurs at the C-cluster, a complicated Ni−Fe−S cluster with a *cubanoid* geometry which is of principal interest in this work. Both clusters represent substantial challenges in the synthesis of weak-field heterometal clusters that are analogues of native clusters in biology.[8]

Shown in Figure 1 are X-ray structures of three C-clusters from different organisms. All contain a $NiFe_4(\mu_3\text{-}S)_4$ core with distorted tetrahedral iron sites, among which is an iron atom with apparent $Fe(\mu_2\text{-}S)(\mu_3\text{-}S)(S_{Cys})(N_{His})$ coordination that is positioned exo to the cubanoid $NiFe_3S_4$ portion of the core. The structures differ mainly in the coordination around nickel. The dithionite-reduced cluster of *Ch* CODH II,[9] recently reported at 1.12 Å resolution[10] after an initial determination at 1.63 Å,[11] is the most accurately determined structure. This cluster features planar NiS_4 coordination and a tetrahedral exo iron atom connected to the $NiFe_3S_4$ portion by one μ_2-S and one μ_3-S* bridge. The two structures of the *Mt* CODH cluster include the exo iron atom but lack the μ_2-S bridge interaction.[4,5] The 1.9 Å structure has been modeled with a CO ligand and distorted tetrahedral coordination at the nickel site.[5] The C-cluster of *Rr* is interpreted in terms of a $\mu_2\text{-}S_{Cys}$ bridge and carries an unidentified ligand at the nickel site. Several of these structures exhibit partial atom occupancies and disordered positions. Further, evidence exists that treatment with CO causes structural changes and may be responsible for the absence of the μ_2-S

(1) Ragsdale, S. W.; Kumar, M. *Chem. Rev.* **1996**, *96*, 2515−2539.
(2) Lindahl, P. A. *Biochemistry* **2002**, *41*, 2097−2105.
(3) Grahame, D. A. *Trends Biochem. Sci.* **2003**, *28*, 221−224.
(4) Doukov, T. I.; Iverson, T. M.; Seravalli, J.; Ragsdale, S. W.; Drennan, C. L. *Science* **2002**, *298*, 567−572.
(5) Darnault, C.; Volbeda, A.; Kim, E. J.; Legrand, P.; Vernède, X.; Lindahl, P. A.; Fontecilla-Camps, J. C. *Nature Struct. Biol.* **2003**, *10*, 271−279.
(6) Bramlett, M. R.; Tan, X.; Lindahl, P. A. *J. Am. Chem. Soc.* **2003**, *125*, 9316−9317.
(7) Seravalli, J.; Xiao, Y.; Gu, W.; Cramer, S. P.; Antholine, W. E.; Krymov, V.; Gerfern, G. J.; Ragsdale, S. W. *Biochemistry* **2004**, *43*, 3944−3955.
(8) Lee, S. C.; Holm, R. H. *Proc. Natl. Acad. Sci. U.S.A.* **2003**, *100*, 3595−3600.
(9) Abbreviations are given in Chart 1.
(10) Dobbek, H.; Svetlitchnyi, V.; Liss, J.; Meyer, O. *J. Am. Chem. Soc.* **2004**, *126*, 5382−5387.
(11) Dobbek, H.; Svetlitchnyi, V.; Gremer, L.; Huber, R.; Meyer, O. *Science* **2001**, *293*, 1281−1285.

10.1021/ja052381s CCC: $30.25

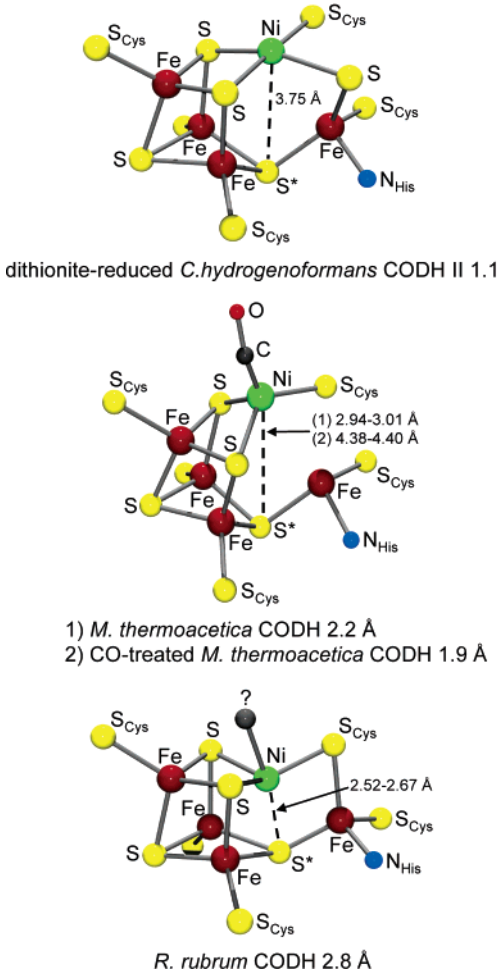

Figure 1. Crystallographic structures of the C-clusters in enzymes from three organisms determined at the indicated resolutions. The axial Ni···S* distances are calculated from coordinates in the Protein Data Base; ranges apply to cases with inequivalent clusters. A CO ligand modeled at nickel is included, and a possible persulfide ligand at iron is omitted in *Mt* CODH (2).

bridge in the *Mt* and *Rr* C-cluster structures.[10,12] Nonetheless, certain constant core structural features have emerged that serve as a basis for synthetic approaches to the C-cluster.

We proceed on the basis that the C-cluster of *Ch* CODH II is the best current definition of the biological structure. Dobbek et al.[10] conclude that the μ_2-S bridge is necessary for activity; hence, the depicted cluster is functional. We note the dissenting interpretation by Feng and Lindahl[13] which, however, is difficult at present to translate into a definite structural objective. The results of nickel K-edge X-ray absorption spectroscopy of the cluster are consistent with a $Ni^{II}S_4$ coordination unit and a bond distance of 2.20 Å.[12] The cluster structures depicted in Figure 1 are designated as cubanoid rather than cubane-type because the axial Ni···S* separation in each is much longer than the 2.2−2.3 Å distances found in authentic $NiFe_3S_4$ cubanes containing tetrahedral Ni^{II}.[14,15] In planar complexes, Ni^{II}−S bond lengths to anionic ligands fall in the 2.10−2.25 Å range.

Cubane-type clusters are potential precursors to the C-cluster structure. Achievement of that structure may be formulated in two steps: (i) creation of a planar Ni^{II} site within the $NiFe_3S_4$ core, and (ii) introduction of a tetrahedral $Fe^{II,III}$ site with appropriate bridges exo to the core in (i) to generate, ideally, the complete $NiFe_4S_5$ core.

In initial experiments directed at step (i), we demonstrated the occurrence of reaction 1.[16] Here a $NiFe_3S_4$ cubane-type

$$[(Ph_3P)NiFe_3S_4(LS_3)]^{2-} + \text{dmpe} \rightarrow [(\text{dmpe})NiFe_3S_4(LS_3)]^{2-} + Ph_3P \quad (1)$$

cluster supported by the semirigid trithiolate ligand LS_3[17] reacts with a chelating diphosphine in a ligand substitution process, resulting in the conversion from a tetrahedral paramagnetic Ni^{II}-PS_3 to a planar diamagnetic $Ni^{II}P_2S_2$ configuration. In the process, the $[NiFe_3S_4]^+$ core changes from an $S = {}^3/_2$ to an $S = {}^5/_2$ ground state. The $NiFe_3S_4$ portion of the product cluster is cubanoid inasmuch as the axial Ni···S* separations in independent clusters are 2.60−2.90 Å.[16]

While the product cluster of reaction 1 lacks the exo iron atom and contains a nonphysiological ligand, it resembles a C-cluster by the integration of planar Ni^{II}, with an accompanying long Ni···S* distance, into a $NiFe_3S_4$ unit. This unit, with planar Ni^{II} in the best defined case, is a constant structural component of C-clusters. The present investigation and that preceding it[16] disclose our current approach to C-cluster synthetic analogues. In this work, we address more generally the ligand substitution chemistry of tetrahedral Ni^{II} in a cubane-type cluster, provide other reactions leading to the formation of planar sites in cubanoid clusters, and document certain substitution reactions of cubane-type Fe_4S_4 clusters. Related research in this laboratory is directed toward the attainment of analogues of the A-cluster of bifunctional CODH.[18,19]

Experimental Section

Preparation of Compounds. All reactions and manipulations were performed under a pure dinitrogen atmosphere using either Schlenk techniques or an inert atmosphere box. Solvents were passed through an Innovative Technology solvent purification system prior to use. Volume reduction and drying steps were carried out in vacuo. Because of the small scale of the preparations, compounds were not analyzed. Those in Table 1 were characterized by X-ray structure determinations. In addition, all clusters display sharp, isotropically shifted ^{1}H NMR spectra. In conjunction with an extensive data set for complexes of the types $[L'NiFe_3S_4(LS_3)]^{z}$ [16,17] and $[Fe_4S_4(LS_3)L']^{z}$ [20−24] obtained in this laboratory, the spectra allow detection of reaction products and establishment of the identity and satisfactory purity of isolated compounds. Selected clusters **12**, **13**, and **16** were also verified by electrospray mass spectrometry. Spectra of species corresponding to

(12) Gu, W.; Seravalli, J.; Ragsdale, S. W.; Cramer, S. P. *Biochemistry* **2004**, *43*, 9029−9035.
(13) Feng, J.; Lindahl, P. A. *J. Am. Chem. Soc.* **2004**, *126*, 9094−9100.
(14) Ciurli, S.; Ross, P. K.; Scott, M. J.; Yu, S.-B.; Holm, R. H. *J. Am. Chem. Soc.* **1992**, *114*, 5415−5423.
(15) Zhou, J.; Scott, M. J.; Hu, Z.; Peng, G.; Münck, E.; Holm, R. H. *J. Am. Chem. Soc.* **1992**, *114*, 10843−10854.
(16) Panda, R.; Zhang, Y.; McLauchlan, C. C.; Rao, P. V.; Tiago de Oliveira, F. A.; Münck, E.; Holm, R. H. *J. Am. Chem. Soc.* **2004**, *126*, 6448−6459.
(17) Zhou, J.; Raebiger, J. W.; Crawford, C. A.; Holm, R. H. *J. Am. Chem. Soc.* **1997**, *119*, 6242−6250.
(18) Rao, P. V.; Bhaduri, S.; Jiang, J.; Holm, R. H. *Inorg. Chem.* **2004**, *43*, 5833−5849.
(19) Rao, P. V.; Bhaduri, S.; Jiang, J.; Hong, D.; Holm, R. H. *J. Am. Chem. Soc.* **2005**, *127*, 1933−1945.
(20) Weigel, J. A.; Holm, R. H. *J. Am. Chem. Soc.* **1991**, *113*, 4184−4191.
(21) Ciurli, S.; Carrié, M.; Weigel, J. A.; Carney, M. J.; Stack, T. D. P.; Papaefthymiou, G. C.; Holm, R. H. *J. Am. Chem. Soc.* **1990**, *112*, 2654−2664.
(22) Zhou, C.; Holm, R. H. *Inorg. Chem.* **1997**, *36*, 4066−4077.
(23) Liu, H. Y.; Scharbert, B.; Holm, R. H. *J. Am. Chem. Soc.* **1991**, *113*, 9529−9539.
(24) Stack, T. D. P.; Holm, R. H. *J. Am. Chem. Soc.* **1988**, *110*, 2484−2494.

Table 1. Crystallographic Data and Structural Refinement Parameters for Compounds Containing Clusters **3**, **12**, **13**, **16**, and **17**[a]

	$(Et_4N)_2$[**3**]·1.5Et_2O	$(Et_4N)_2$[**12**]·1.25MeCN·0.25Et_2O	$(Et_4N)_2$[**13**]·1.5MeCN	$(Et_4N)_2$[**16**]·2MeCN	$(Et_4N)_2$[**17**]·0.5MeCN
formula	$C_{76}H_{109}Fe_3N_2NiO_{1.5}PS_{13}$	$C_{76.5}H_{107.25}Fe_3N_{3.25}O_{0.25}P_2Pd_1S_{13}$	$C_{76}H_{105.5}Fe_3N_{3.5}P_2Pt_1S_{13}$	$C_{75}H_{101}Fe_4N_5S_{14}$	$C_{82}H_{100.5}Fe_4N_{2.5}OP_1S_{14}$
fw	1749	1829	1910	1745	1840
cryst system	monoclinic	triclinic	triclinic	monoclinic	triclinic
space group	$P2_1/c$	$P\bar{1}$	$P\bar{1}$	$P2_1/c$	$P\bar{1}$
Z	4	4	4	8	2
a, Å	16.301(2)	18.258(3)	18.256(4)	23.945(4)	12.847(3)
b, Å	20.044(3)	18.942(4)	19.011(5)	34.261(6)	13.073(3)
c, Å	27.789(4)	27.283(4)	27.376(8)	22.480(4)	29.484(6)
α, deg	90	78.38(2)	78.80(1)	90	87.695(4)
β, deg	95.832(3)	88.96(1)	89.16(4)	111.899(4)	83.999(4)
γ, deg	90	81.98(1)	81.83(2)	90	62.947(4)
V, Å^3	9033(2)	9152(3)	9225(4)	17111(5)	4386(2)
GOF (F^2)	1.046	0.944	1.019	1.159	1.053
R_1,[b] wR_2[c]	0.0696, 0.1831	0.0720, 0.1589	0.0519, 0.1454	0.0865, 0.2036	0.0451, 0.1152

[a] Collected using Mo Kα radiation ($\lambda = 0.71073$) at $T = 213$ K. [b] $R(F_o) = \sum[(F_o - F_o)]/\sum(F_o)$. [c] $R_w(F_o^2) = \{\sum[w(F_o^2 - F_c^2)^2/\sum[w(F_o^2)^2]\}^{1/2}$.

$\{M^{2-} + H^+\}^-$ displayed isotope patterns in excellent agreement with calculated values.

$(Et_4N)_2$[(Bu^tNC)$NiFe_3S_4(LS_3)$] ($(Et_4N)_2$[2]). To a solution of $(Et_4N)_3$-$[Fe_3S_4(LS_3)]$[25] (100 mg, 61.2 μmol) in 25 mL of acetonitrile was added a solution of $[Ni(CNBu^t)_4]$[26] (28.7 mg, 73.4 μmol) in 5 mL of acetonitrile. The solution was stirred for 2 h, and the solvent was removed to leave a dark brown solid. The solid was washed with ether (5 mL) and dried to afford the product as 94 mg (93%) of a brown solid. ^{1}H NMR (CD_3CN, anion): δ 14.34 (5-H); 12.04, 8.81 (6-Me, 4-Me); 7.46, 6.25 (2′-H, 3′-H); 2.30 (4′-Me), 0.88 (Bu^t).

$(Et_4N)_2$[(Me_3P)$NiFe_3S_4(LS_3)$] ($(Et_4N)_2$[3]). To a solution of $(Et_4N)_2$-$[(Bu^tNC)NiFe_3S_4(LS_3)]$ (25.0 mg, 15.2 μmol) in 4 mL of acetonitrile was added 18.2 μL of a 1 M solution of Me_3P in toluene. The solution was stirred for 1 h and filtered through Celite. Slow diffusion of ether into the filtrate gave the product as 13 mg (54%) of a black crystalline solid. ^{1}H NMR (CD_3CN, anion): δ 39.6 (Me_3P), 14.38 (5-H); 11.76, 8.59 (6-Me, 4-Me); 7.39, 6.21 (2′-H, 3′-H); 2.28 (4′-Me).

$(Et_4N)_2$[(dmpe)$NiFe_3S_4(LS_3)$] ($(Et_4N)_2$[9]). To a solution of $(Et_4N)_3$-$[Fe_3S_4(LS_3)]$ (100 mg, 61.2 μmol) in 16 mL of acetonitrile was added a suspension of $[Ni(cod)_2]$ (18.5 mg, 67.3 μmol) in 4 mL of DMF, followed by the addition of dmpe (11.2 μL, 67.3 μmol). The reaction mixture was stirred for 4 h and filtered, and the filtrate was taken to dryness in vacuo. The black solid was washed with ether (3 × 5 mL) and dried in vacuo. This material was recrystallized from acetonitrile/DMF (5:1 v/v) by means of vapor diffusion of ether to afford the product as 45 mg (43%) of black needles. The ^{1}H NMR spectrum of this material is identical to that of authentic $[(dmpe)NiFe_3S_4(LS_3)]^{2-}$ prepared by a different method.[16]

$(Et_4N)_2$[(dmpe)$PdFe_3S_4(LS_3)$] ($(Et_4N)_2$[12]). To a solution of $(Et_4N)_3$-$[Fe_3S_4(LS_3)]$ (100 mg, 61.2 μmol) in 18 mL of acetonitrile was added a suspension of $[Pd(dba)_2]$ (42.2 mg, 73.4 μmol) in 1.5 mL of Me_2SO, followed by the addition of dmpe (12.3 μL, 73.4 μmol). The reaction mixture was stirred for 3 h and filtered. Vapor diffusion of ether into the filtrate afforded the pure product as 74.0 mg (69%) of black needles. Mass spectrum: m/z 1500.0 (calcd for $\{M^{2-} + H^+\}^-$, 1499.9). ^{1}H NMR (CD_3CN, anion): δ 19.32 (5-H), 17.01, 13.62 (6-Me, 4-Me); 7.29, 6.49 (2′-H, 3′-H); 2.32 (4′-Me), 1.40 (CH_2-dmpe), 0.92 (Me-dmpe).

$(Et_4N)_2$[(dmpe)$PtFe_3S_4(LS_3)$] ($(Et_4N)_2$[13]). To a solution of $(Et_4N)_3$-$[Fe_3S_4(LS_3)]$ (50 mg, 30.6 μmol) in 8 mL of acetonitrile was added a suspension of $[Pt(PPh_3)_4]$ (41.0 mg, 33.0 μmol) in 1.5 mL of DMF, followed by the addition of dmpe (5.5 μL, 33.0 μmol). The reaction mixture was stirred for 3 h and filtered. Vapor diffusion of ether into the filtrate afforded the pure product as 21.0 mg (38%) of black needles. Mass spectrum: m/z 1587.4 (calcd for $\{M^{2-} + H^+\}^-$, 1587.8). ^{1}H NMR (CD_3CN, anion): δ 16.97 (5-H), 16.25, 13.40 (6-Me, 4-Me); 7.34, 6.59 (2′-H, 3′-H); 2.35 (4′-Me), 2.27 (CH_2-dmpe), 0.03 (Me-dmpe).

$(Et_4N)_2$[$Fe_4S_4(LS_3)(SCH_2CH_2PPh_2)$] ($(Et_4N)_2$[15]). To a solution of $(Bu_4N)_2[Fe_4S_4(LS_3)Cl]$[22] (136 mg, 75.0 μmol) in 20 mL of acetonitrile was added a suspension of $NaSCH_2CH_2PPh_2$[27] (20 mg, 75.0 μmol) in 5 mL of acetonitrile. The mixture was stirred for 2 h and filtered into a solution of $(Et_4N)(PF_6)$ (42.0 g, 150 μmol), and that mixture was stirred for 30 min. Ether was layered onto the solution at −20 °C, causing separation of the product as 102 mg (76%) of a dark brown solid. ^{1}H NMR (CD_3CN, anion): δ 12.05 (SCH_2), 8.16 (5-H); 7.96, 7.85, 7.53 (Ph); 7.14, 6.84 (2′-H, 3′-H); 5.10 (br, 2-H); 3.83, 3.73 (6-Me, 4-Me); 2.24 (4′-H), 2.10 (CH_2P). Mössbauer spectrum (4.2 K): $\delta = 0.44$ mm/s, $\Delta E_Q = 1.14$ mm/s. $E_{1/2} = -0.47$ V (1−/2−), −1.11 V (2−/3−) (acetonitrile).

$(Bu_4N)_2$[$Fe_4S_4(LS_3)(SCH_2CH_2PPh_2)$] ($(Bu_4N)_2$[15]). To a solution of $(Bu_4N)_2[Fe_4S_4(LS_3)Cl]$ (400 mg, 0.220 mmol) in 80 mL of acetonitrile was added a suspension of $NaSCH_2CH_2PPh_2$ (59 mg, 0.22 mmol) in 10 mL of acetonitrile. The mixture was stirred for 2 h and filtered through Celite, and the solvent was removed in vacuo. The product was obtained as 0.365 g (82%) of a glassy black solid. The ^{1}H NMR spectrum of the anion was identical to that from the preceding preparation. Mössbauer spectrum (4.2 K): $\delta = 0.45$ mm/s, $\Delta E_Q = 1.14$ mm/s.

$(Et_4N)_2$[$Fe_4S_4(LS_3)(SCH_2CH_2NMe_2)$] ($(Et_4N)_2$[16]). To a solution of $(Bu_4N)_2[Fe_4S_4(LS_3)Cl]$ (52 mg, 29 μmol) in 10 mL of acetonitrile was added a suspension of $NaSCH_2CH_2NMe_2$ (3.6 mg, 29 μmol) in 5 mL of acetonitrile. The mixture was stirred for 2 h and filtered into a solution of $(Et_4N)(PF_6)$ (16 mg, 57 μmol), and that mixture was stirred for 30 min. Ether was layered onto the solution at −20 °C, causing separation of the product as 37 mg (80%) of a dark brown solid. Mass spectrum: m/z 1402.9 (calcd for $\{M^{2-} + H^+\}^-$, 1402.8). Mössbauer spectrum (4.2 K): $\delta = 0.45$ mm/s, $\Delta E_Q = 1.14$ mm/s. ^{1}H NMR (CD_3CN, anion): δ 20.90 (SCH_2), 8.23 (5-H), 7.15, 6.76 (2′-H, 3′-H); 6.85 (NMe_2), 5.00 (2-H), 3.89, 3.64 (6-Me, 4-Me); 2.26 (4′-Me), 2.12 (CH_2N). $E_{1/2} = -0.16$ V (1−/2−), −1.14 V (acetonitrile).

$(Bu_4N)_2$[$Fe_4S_4(LS_3)(SCH_2CH_2NMe_2)$] ($(Bu_4N)_2$[16]). To a solution of $(Bu_4N)_2[Fe_4S_4(LS_3)Cl]$ (200 mg, 0.110 mmol) in 40 mL of acetonitrile was added a suspension of $NaSCH_2CH_2NMe_2$ (14 mg, 0.11 mmol) in 5 mL of acetonitrile. The mixture was stirred for 3 h and filtered through Celite, and the solvent was removed in vacuo. The black solid was dissolved in 20 mL of acetonitrile, the solution was filtered, and the filtrate was layered with ether. The solid which separated was washed with ether and dried in vacuo to afford the product as 160 mg (77%) of a glassy black solid. Mössbauer spectrum (4.2 K): $\delta = 0.45$ mm/s, $\Delta E_Q = 1.13$ mm/s. Mass spectrum: m/z

(25) Zhou, J.; Hu, Z.; Münck, E.; Holm, R. H. *J. Am. Chem. Soc.* **1996**, *118*, 1966−1980.
(26) Ittel, S. D. *Inorg. Synth.* **1990**, *28*, 98−104.
(27) Chatt, J.; Dilworth, J. R.; Schmutz, J. A. *J. Chem. Soc., Dalton Trans.* **1979**, 1595−1599.

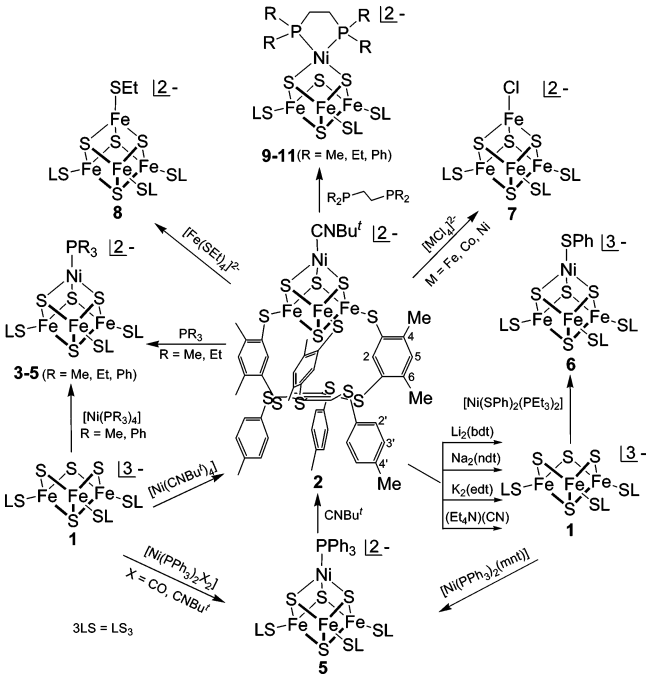

Figure 2. Scheme showing the synthesis and reactions of $[(Bu^tNC)NiFe_3S_4(LS_3)]^{2-}$ (**2**) from $[Fe_3S_4(LS_3)]^{3-}$ (**1**) leading to $[NiFe_3S_4]^{+}$ (**3**−**6**, **9**−**11**) and $[Fe_4S_4]^{2+}$ clusters (**7**, **8**); note the LS_3 ligand numbering scheme.

1402.6 ($\{M^{2-} + H^{+}\}^{-}$). The ^{1}H NMR spectrum of the anion was identical to that of the preceding preparation.

Generation of Clusters in Solution. A series of clusters of the type $[L'NiFe_3S_4(LS_3)]^{2-,3-}$ were prepared in situ by the substitution reactions of $[(Bu^tNC)NiFe_3S_4(LS_3)]^{2-}$ summarized in Figure 2. In a typical experiment, a known amount of reactant (1.0−1.1 equiv) as a solution or suspension in CD_3CN was added to a ca. 10 mM solution of starting cluster in CD_3CN. Product identity was established by ^{1}H NMR spectroscopy. The compounds bicyclo[2.2.1]hepta-*exo*-*cis*-2,3-dithiol,[28] $Ph_2PCH_2CH_2SH$,[27] $(Et_4N)_2[(Ph_3P)NiFe_3S_4(LS_3)]$,[17] $[Ni(PPh_3)_2(Bu^t-NC)_2]$,[29] $[Ni(PMe_3)_4]$,[26] $(Et_4N)_2[Fe(SEt)_4]$,[30] $[Ni(PPh_3)_2(mnt)]$,[31] $(Et_4N)[MCl_4]$ (M = Fe, Co, Ni),[32] and $[Ni(SPh)_2(PEt_3)_2]$[33] were prepared as described. Other compounds were commercial samples. Similar experiments were conducted in acetonitrile with $[(Ph_3P)NiFe_3S_4(LS_3)]^{2-}$ or $[(Bu^tNC)NiFe_3S_4(LS_3)]^{2-}$ and the sodium salts of $Ph_2PCH_2CH_2SH$, $Me_2PCH_2CH_2SH$,[34] 1,2-$Ph_2PC_6H_4SH$,[35] and $Me_2NCH_2CH_2SH$ (see text).

In the following sections, clusters are designated numerically as in Chart 1.

X-ray Structure Determinations. The structures of the five compounds listed in Table 1 were determined. Suitable crystals were obtained by ether diffusion ($(Et_4N)_2$[**3**]·0.5MeCN, $(Et_4N)_2$[**12**]·1.25MeCN·0.25Et_2O, $(Et_4N)_2$[**13**]·1.5MeCN) and hexane diffusion ($(Et_4N)_2$[**16**]·2MeCN) into acetonitrile solutions. The phosphine oxide compound $(Et_4N)_2$[**17**]·0.5MeCN was formed during the attempted crystallization of **15** from acetonitrile. Data for crystals containing **3**, **16**, and **17** were collected on a Siemens (Bruker) SMART CCD-based diffractometer. Data for crystals containing **12** and **13** were obtained with a Siemens (Bruker) APEX CCD diffractometer. Cell parameters were retrieved using SMART software and refined with SAINT on all observed reflections. Data were collected using 0.3° intervals in ϕ and ω for 30 s/frame such that a hemisphere of data was collected. A total of 1270 frames was collected with a maximum resolution of 0.75 Å. The first 50 frames were re-collected at the end of the data collection to monitor for decay; none was found. The highly redundant data sets were reduced using SAINT and corrected for Lorentz and polarization effects. Absorption corrections were applied with SADABS. Structures were solved by direct methods using SHELXL-97. The positions of the metal atoms and coordinated atoms were located from direct-methods *E*-maps; other non-hydrogen atoms were found in alternating difference Fourier syntheses and least-squares refinement cycles. These atoms were refined anisotropically during the final cycles. Hydrogen atoms were placed in calculated positions and refined as riding atoms with a uniform value of U_{iso}. Crystallographic data are collected in Table 1.[37]

Chart 1. Designation of Clusters and Abbreviations Used Herein

$[Fe_3S_4(LS_3)]^{3-}$	**1**[25]
$[(Bu^tNC)NiFe_3S_4(LS_3)]^{2-}$	**2**
$[(R_3P)NiFe_3S_4(LS_3)]^{2-}$	R = Me **3,** Et **4**, Ph **5**[17]
$[(PhS)NiFe_3S_4(LS_3)]^{3-}$	**6**
$[Fe_4S_4(LS_3)Cl]^{2-}$	**7**[24]
$[Fe_4S_4(LS_3)(SEt)]^{2-}$	**8**[36]
$[(dmpe)NiFe_3S_4(LS_3)]^{2-}$	**9**[16]
$[(R_2PCH_2CH_2PR_2)NiFe_3S_4(LS_3)]^{2-}$	R = Et **10**, Ph **11**
$[(dmpe)PdFe_3S_4(LS_3)]^{2-}$	**12**
$[(dmpe)PtFe_3S_4(LS_3)]^{2-}$	**13**
$[[Fe_4S_4(LS_3)(PMe_3)]^{1-}$	**14**
$[Fe_4S_4(LS_3)(SCH_2CH_2PPh_2)]^{2-}$	**15**
$[Fe_4S_4(LS_3)(SCH_2CH_2NMe_2)]^{2-}$	**16**
$[Fe_4S_4(LS_3)(SCH_2CH_2P(O)Ph_2)]^{2-}$	**17**

bdt = benzene-1,2-dithiolate(2-), *Ch*, *Carboxydothermus hydrogenoformans*; CODH; cod, 1,5-cyclooctadiene, dba, dibenzylideneacetone, CODH, carbon monoxide dehydrogenase; dmpe = bis(1,2-dimethylphosphino)ethane, edt = ethane-1,2-dithiolate(2-), LS_3 = 1,3,5-tris((4,6-dimethyl-3-mercaptophenyl)thio)-2,4,6-tris(*p*-tolylthio)benzene(3-), 3LS = LS_3; mes = mesityl; mnt = maleonitriledithiolate(2-), *Mt*, *Moorella thermoacetica*; ndt = bicyclo[2.2.1]hepta-*exo*-*cis*-2,3-dithiolate(2-); *Rr*, *Rhodospirillum rubrum*

Other Physical Measurements. ^{1}H NMR spectra were obtained with a Bruker AM-400 spectrometer. Electrochemical measurements were carried out with a PAR model 263 potentiostat/galvanostat using a Pt working electrode and 0.1 M $(Bu_4N)(ClO_4)$ supporting electrolyte; potentials are referred to the SCE. Electrospray ionization mass spectra were recorded on a LCT mass spectrometer. Mössbauer spectra were collected with a constant acceleration spectrometer. Data were analyzed using WMOSS software (Web Research Inc., Edina, MN); isomer shifts are referenced to iron metal at room temperature. Magnetic measurements were made with a Quantum Design MPMS-XL SQUID magnetometer (Texas A&M University).

Results and Discussion

The closest synthetic approach to the C-clusters are $NiFe_3(\mu_3\text{-}S)_4$ cubane-type clusters with tetrahedral metal sites; methods of synthesis have been summarized.[16] All isolated clusters of this type contain the $[NiFe_3S_4]^{+}$ core. The oxidation states $[NiFe_3S_4]^{2+,0}$ have been detected electrochemically but not isolated.[14,15,17]

Synthesis and Reactions of $NiFe_3S_4$ Cubane-Type Clusters. Relevant reactions are summarized in Figure 2. In certain cases (**5**, **7**−**9**), clusters were isolated in this or past work; in all other reactions, cluster formation in situ was detected by isotropically shifted ^{1}H NMR spectra characteristic of the core oxidation state.

(28) Shields, T. C.; Kurtz, A. N. *J. Am. Chem. Soc.* **1969**, *91*, 5415−5416.
(29) Wenschuh, E.; Wilhelm, D.; Hartung, H.; Baumeister, U. *Z. Anorg. Allg. Chem.* **1994**, *620*, 2048−2052.
(30) Hagen, K. S.; Watson, A. D.; Holm, R. H. *J. Am. Chem. Soc.* **1983**, *105*, 3905−3913.
(31) Davison, A.; Edelstein, N.; Holm, R. H.; Maki, A. H. *Inorg. Chem.* **1964**, *3*, 814−823.
(32) Gill, N. S.; Taylor, F. B. *Inorg. Synth.* **1967**, *9*, 136−142.
(33) Yamamoto, T.; Sekine, Y. *Inorg. Chim. Acta* **1984**, *83*, 47−53.
(34) Kita, M.; Yamamoto, T.; Kashiwabara, K.; Fujita, J. *Bull. Chem. Soc. Jpn.* **1992**, *65*, 2272−2274.
(35) Block, E.; Ofori-Okai, G.; Zubieta, J. *J. Am. Chem. Soc.* **1989**, *111*, 2327−2329.
(36) Cai, L.; Holm, R. H. *J. Am. Chem. Soc.* **1994**, *116*, 7177−7188.

(37) See paragraph at the end of this article for Supporting Information available.

(a) Reactions Based on Cuboidal Cluster 1. The synthetic procedure utilized here for $NiFe_3S_4$ clusters with *tetrahedral* Ni^{II} sites is metal incorporation into the cuboidal $[Fe_3S_4]^0$ core of cluster **1**,[17] which is stabilized by tridentate LS_3.[24] The ideal minimal reaction of cluster formation is the inner-sphere redox process 2, leading to a cluster whose Ni^{2+} ($S = 1$) + $[Fe_3S_4]^-$ ($S = {}^5/_2$) components are antiferromagnetically coupled to give cluster spin $S = {}^3/_2$.[14,15] However, the same oxidation state occurs in **5** and **6**, which are formed from Ni^{2+} complexes by reactions in which it is likely that the anionic sulfur ligands act as one-electron reductants.

$$[Fe_3S_4]^0 + Ni^+ \rightarrow [NiFe_3S_4]^+ \quad (2)$$

$$[Fe_3S_4]^0 + M^0 \rightarrow [MFe_3S_4]^+ + e^- \quad (3)$$

Further, in minimal reaction 3, Ni^0 complexes afford phosphine clusters **3**−**5** and isonitrile cluster **2**, isolated in 93% yield. Because potentials of the couples $[(Ph_3P)NiFe_3S_4(SR)_3]^{2-/3-}$ are highly reducing (ca. −1.6 V vs SCE),[15,17] it is probable that any $[NiFe_3S_4]^0$ cluster formed is adventiously oxidized or not formed at all. The disposition of the additional electron is unknown. These observations and others that follow collectively are indicative of the preferential stability of the $[NiFe_3S_4]^+$ oxidation state.

To obtain a representative structure of an $[NiFe_3S_4]^+$ cluster supported by the LS_3 ligand, the structure of phosphine cluster **3**, shown in Figure 3, was determined. Metric parameters are collected in Table 2. The cluster, with alternating coordinating arms above (*a*) and buttressing S-*p*-tolyl legs below (*b*) the central benzene ring in the conformation *ababab*, has idealized trigonal symmetry. The bottom of the core at S4 is placed at 3.79(2) Å above the central ring. Tetrahedral stereochemistry at the $Ni^{II}PS_3$ site is made evident by the angles P−Ni−S = 104.7(1)−118.4(1)° and S−Ni−S = 105.41(9)−106.03(9)°. The Me_3P ligand is bound at 2.204(3) Å from the Ni^{II} atom. Note the mean Ni−S distance of 2.263(6) Å. These dimensions compare closely with those of $[(Ph_3P)NiFe_3S_4(Smes)_3]^-$.[15] Other bond distances and angles are unexceptional.

(b) Reactions at the Ni^{II} Site. Cluster **2** was selected to examine reactions at the Ni^{II} site. The ^1H NMR spectra of **2** and **3** in Figure 4 illustrate the well-resolved isotropically shifted spectra induced by the $[NiFe_3S_4]^+$ ($S = {}^3/_2$) oxidation state bound to LS_3. In addition to its formation from **1** and $[Ni(CNBu^t)_4]$, **2** can be obtained by treatment of **5** with 1.1 equiv of the isonitrile. An excess of ligand affords a mixture of **2** and previously reported $[Fe_4S_4(LS_3)(Bu^tNC)_3]^-$, containing a low-spin six-coordinate Fe^{II} site.[38] Treatment of **2** with $[FeCl_4]^{2-}$ and $[Fe(SEt)_4]^{2-}$ led to nickel removal and formation of **7** and **8**, respectively. Reaction with $[MCl_4]^{2-}$ (M = Co, Ni) also led to **7**; no evidence for formation of heterometal clusters was obtained. The outcome of these reactions, which must involve cluster disassembly and re-formation, is another indication of the stability of the $[Fe_4S_4]^{2+}$ core relative to those containing heterometals. Reactions of **2** with the chelating ligands bdt, edt, and ndt were intended to introduce low-spin Ni^{II} dithiolate sites; however, these reagents or cyanide removed Ni^{II} with formation of **1**.

(38) Weigel, J. A.; Srivastava, K. K. P.; Day, E. P.; Münck, E.; Holm, R. H. *J. Am. Chem. Soc.* **1990**, *112*, 8015−8023.

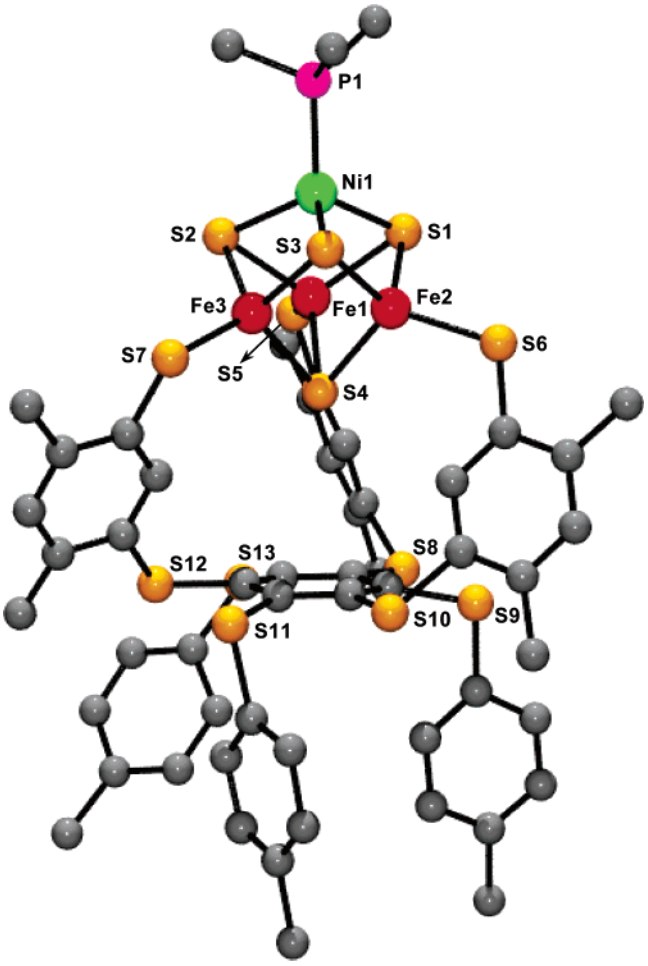

Figure 3. Structure of $[(Me_3P)NiFe_3S_4(LS_3)]^{2-}$ with partial atom labeling scheme. The ligand has the *ababab* conformation.

Clusters with Planar M^{II} Sites. (a) Synthesis. The desired *planar* Ni^{II} site is formed in clusters **9**−**11** from **2** and chelating diphosphines in ligand substitution reactions analogous to reaction 1. By imposition of a strong in-plane ligand field, these reactions result in the transformation of tetrahedral to planar Ni^{II} with retention of all core atoms. Conversions to the product clusters in situ are ≳90%. Reactions are indicated by the appearance of the free isonitrile resonance and the characteristic spectra of the product clusters (see below). Further experimentation directed toward planar sites led to the development of the metal incorporation reactions in Figure 5. These reactions are of type 3 (M = Ni, Pd, Pt) and afford the clusters **9**, **12**, and **13**, which were isolated in moderate yields as Et_4N^+ salts (**9**, 43%; **12**, 69%; **13**, 38%). While the reactants are potential two-electron reductants, clusters containing $[MFe_3S_4]^+$ cores were obtained in all cases. In this and other work, we have found without exception that the use of potential two-electron reductants in metal incorporation reactions results in the delivery of only one electron to the product core. Reactions affording Ni^{II} clusters **9**−**11** by ligand substitution or metal incorporation with accompanying electron transfer are versions of step (i) in the synthesis of the C-cluster. Because metal incorporation into **1** produces a cleaner product on a larger reaction scale than does ligand displacement from **2** or **5**, it is the method of choice for the preparation of cluster **9**.

(b) Structures and Properties. The overall structures of Pd^{II} and Pt^{II} clusters **12** and **13**, respectively, are shown in Figure

Table 2. Selected Interatomic Distances (Å) and Angles (deg) for the Heterometal Clusters $[(Me_3P)NiFe_3S_4(LS_3)]^{2-}$ (**3**) and $[(dmpe)MFe_3S_4(LS_3)]^{2-}$, M = Pd (**12**) and Pt (**13**)

	3[a]	12[b]	13[c]
M−P1	2.204(3)	2.235(4)	2.219(2)
M−P2		2.240(5)	2.230(2)
M−S1	2.260(3)	2.435(4)	2.439(2)
M−S2	2.270(2)	3.017(4)	3.107(3)
M−S3	2.260(2)	2.398(4)	2.394(2)
Fe1−S1	2.291(2)	2.319(4)	2.307(2)
Fe1−S2	2.288(2)		
Fe1−S3		2.278(4)	2.279(2)
Fe1−S4	2.269(2)	2.304(4)	2.295(1)
Fe2−S1	2.266(2)	2.359(4)	2.359(2)
Fe2−S2		2.224(5)	2.233(2)
Fe2−S3	2.290(3)		
Fe2−S4	2.312(2)	2.335(5)	2.328(2)
Fe3−S2	2.281(2)	2.267(5)	2.251(2)
Fe3−S3	2.291(3)	2.379(4)	2.387(2)
Fe3−S4	2.306(2)	2.301(4)	2.309(2)
Fe−SL[d]	2.303(7)	2.332(8)	2.32(2)
S4−ctr[e]	3.79(2)	3.752(4)	3.741(4)
P1−M−P2		86.3(2)	87.00(6)
P1−M−S1	118.4(1)	89.7(2)	89.81(5)
P1−M−S2	115.7(1)		
P1−M−S3	104.7(1)	171.9(2)	174.43(5)
P2−M−S3		86.8(2)	88.00(5)
S1−M−S3	106.03(9)	97.2(1)	95.25(5)
S1−M−S2	105.52(9)		
S2−M−S3	105.41(9)		
Fe2−S2−Fe3		73.6(1)	73.94(5)
MS1S3/Fe2S2Fe3[f]	(α)	23.0(3)	25.85(9)
Fe2S4Fe3/Fe2S2Fe3[f]	(β)	24.2(3)	25.10(9)

[a] M = Ni^{II}. [b] M = Pd^{II}; one of two independent clusters. [c] M = Pt^{II}; one of two independent clusters. [d] Mean value of terminal bond lengths. [e] Distance from S4 to the centroid of the central benzene ring. [f] Dihedral angle.

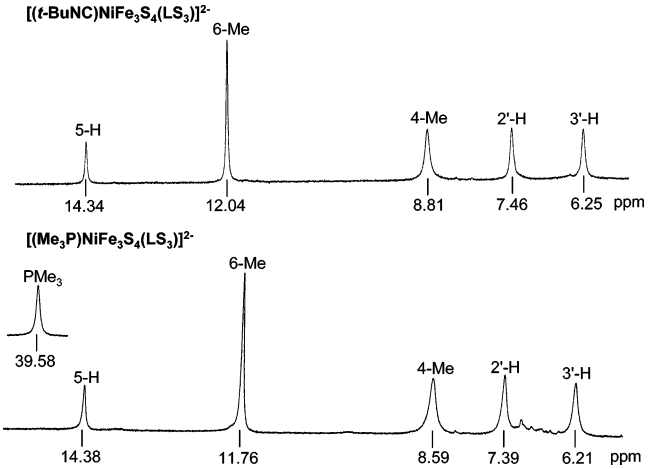

Figure 4. ^1H NMR spectra of $[(Bu^tNC)NiFe_3S_4(LS_3)]^{2-}$ (upper) and $[(Me_3P)NiFe_3S_4(LS_3)]^{2-}$ (lower) in CD_3CN solutions at ~298 K. Signal assignments are indicated. The 4′-Me signals of the isonitrile (δ 2.30) and phosphine (δ 2.28) clusters are not shown.

6; selected bond lengths and angles are collected in Table 2. These species are effectively isostructural with Ni^{II} cluster **9**.[16] The clusters do not achieve congruency owing mainly to the larger radii of Pd^{II} and Pt^{II} and differences in M···S* separations.

The Et_4N^+ salts crystallize with two independent cluster anions, both of which have the *ababab* ligand conformation. The most conspicuous feature of the structures is the presence of planar $M^{II}P_2S_2$ coordination units integrated into the MFe_3S_4 cores. Core structures are presented in more detail in Figure 7. The dihedral angles α and β in Table 2 are such that the planes

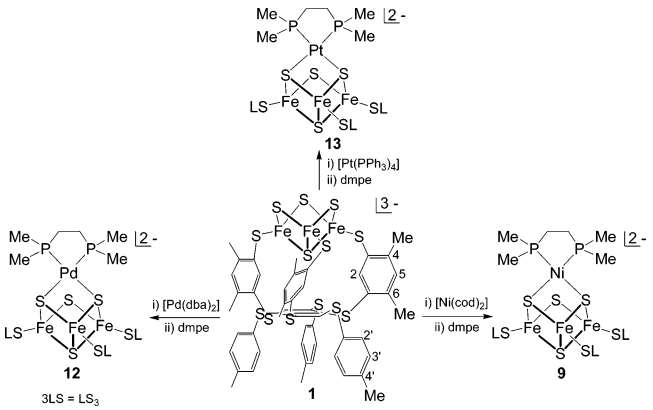

Figure 5. Synthesis of the clusters $[(dmpe)MFe_3S_4(LS_3)]^{2-}$ (M = Ni (**9**), Pd (**12**), Pt (**13**)) from cuboidal $[Fe_3S_4(LS_3)]^{3-}$ (**1**), M^0 reactants, and dmpe.

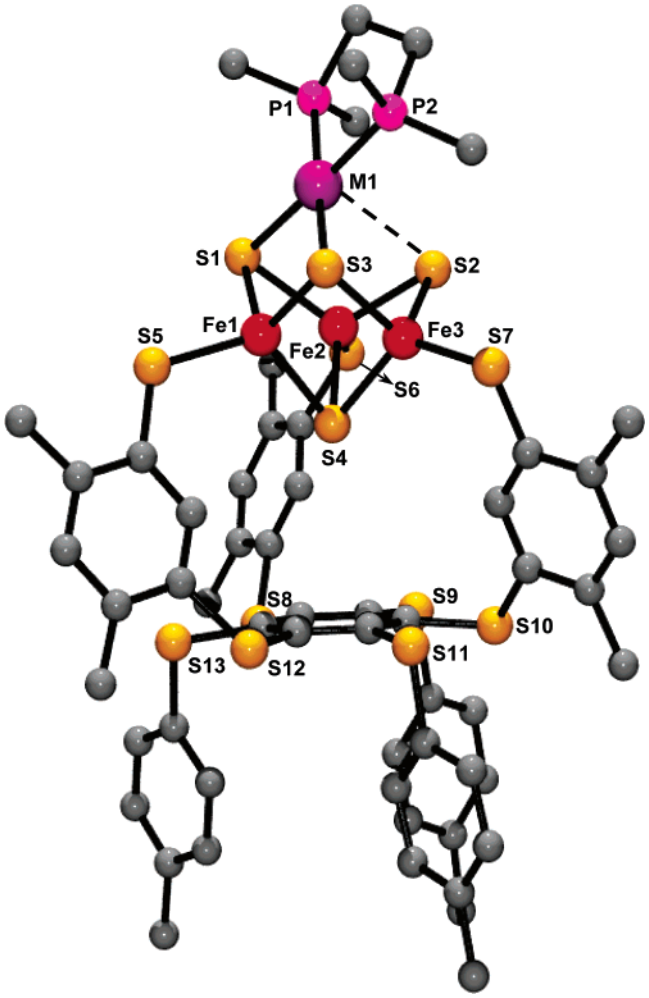

Figure 6. Structure of one of two inequivalent clusters of $[(dmpe)MFe_3S_4(LS_3)]^{2-}$ (M = Pd, Pt) with partial atom labeling schemes. The ligand has the *ababab* conformation.

MS1S3 and Fe2S2Fe3 are folded in opposite directions along the S1···S3 and Fe2···Fe3 directions, respectively. This results in M···S* (S2,S15) axial separations that are much longer than bonded distances (Fe−S4, Fe2−S1, Fe3−S3) that are roughly parallel to the M−S* vector. The M···S* separations of 3.017(4)−3.392(3) Å in **12** and **13**, when considered with the data for **9** (2.602(2)−2.901(2) Å), further accentuate planar coordination and the variability in axial S* atom separations for the metal atom. When assessed against complexes of the general type

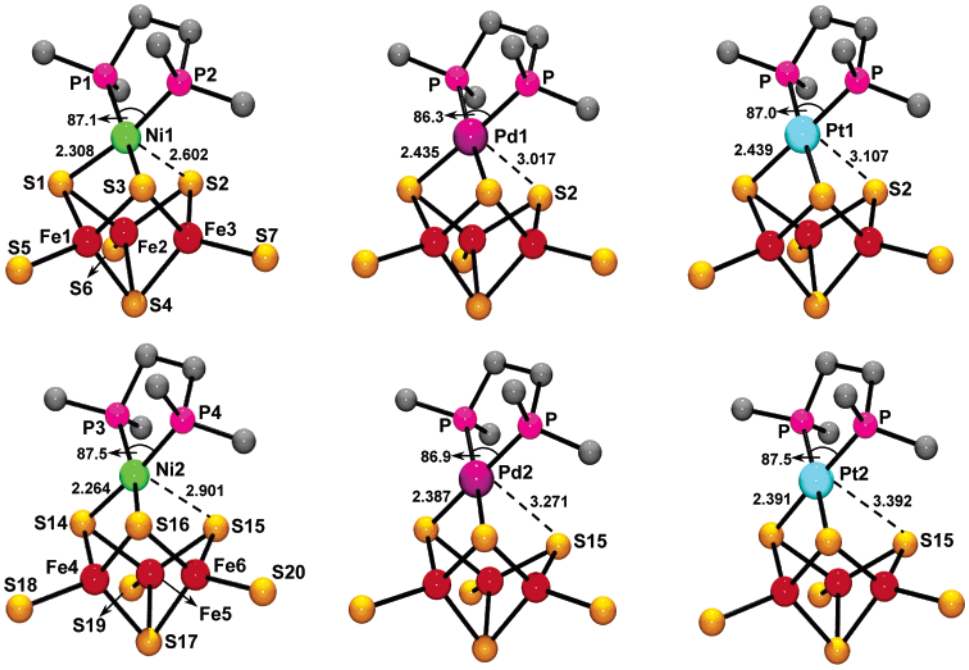

Figure 7. Core structures $[(dmpe)MFe_3S_4]^+$ (M = Ni, Pd, Pt) of two inequivalent clusters within the asymmetric unit showing selected interatomic distances (Å) and angles (deg). The atom numbering schemes of the Ni clusters apply to the Pd and Pt clusters. Note the planar coordination units and the long M···S* (S2/S15) axial separations.

$[M(dppe)(SR)_2]$, with M = Pd^{II} [39−43] and Pt^{II},[43−47] where the pairs of phosphorus and sulfur atoms are necessarily cis as in the clusters, the metric data for **12** and **13** indicate normal planar coordination. The P−M−P bite angles of 84.9−86.8° compare well with the cluster range of 86.3−87.5°, as do the M−P distances 2.25−2.31 Å vs 2.22−2.24 Å for the clusters. Comparison of M−SR bond distances in the complexes (2.30−2.38 Å) and the clusters (2.39−2.44 Å) is less exact owing to the differences in thiolate vs μ_3-S atoms, but the values are commensurate. In the Ni^{II} cluster **9**, the Ni−S distances are ca. 0.05−0.10 Å longer than the normal Ni−SR bonds in planar complexes, a situation arising from the semirigidity of the Fe_3S_4 portion of the core structure. The larger radii of Pd^{II} (0.78 Å) and Pt^{II} (0.74 Å) vs planar Ni^{II} (0.69 Å)[48] may allow an improved fit within the cubanoid core inasmuch as the majority of M−S cluster distances occur near 2.40 Å. Whether this matter contributes to the improved stability of **12** compared to **9** is presently unknown. The Pd^{II} cluster (more extensively handled than **13**) is easier to purify, manipulate, and crystallize than is its Ni^{II} analogue.

Consistent with their close structural relationship, the properties of **9**, **12**, and **13** set out in Table 3 are highly similar. Isomer shifts are nearly identical and correspond to the mean oxidation state $Fe^{2.33+}$. Redox potentials for reduction of the $[MFe_3S_4]^+$ state are indistinguishable; peak potentials for irreversible oxidations show some variability. As illustrated in Figure 8 for **9** and **12**, the $[MFe_3S_4]^+$ oxidation state with planar M^{II} sites, when bound to LS_3, generates a highly characteristic pattern of

Table 3. Mössbauer and Redox Properties of $[(dmpe)MFe_3S_4(LS_3)]^{2-}$ (M = Ni, Pd, Pt)

M	δ (mm/s)[b]	ΔE_Q (mm/s)[b]	$E_{1/2}$ (V)[a] $[MFe_3S_4]^0 \leftrightarrow [MFe_3S_4]^+$	$E_{1/2}$ (V)[a] $[MFe_3S_4]^+ \leftrightarrow [MFe_3S_4]^{2+}$
Ni[c]	0.64	2.72	−1.03[d]	−0.01[e]
	∼0.54	variable[g]		
Pd	0.63	2.54 (1)[h]	−1.02[f]	+0.19[e]
	0.51	1.11 (3)		
Pt	0.63	2.45 (1)	−1.02[f]	+0.11[e]
	0.51	1.16 (3)		

[a] Vs SCE (100 mV/s). [b] 77 K. [c] Reference 16. [d] Acetonitrile. [e] E_{pa} for irreversible process. [f] DMF. [g] Complex spectrum. [h] Relative intensities.

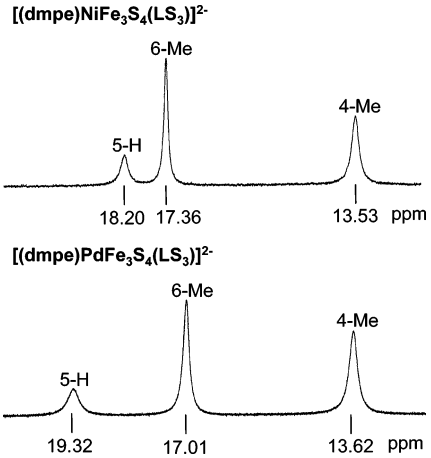

Figure 8. Comparison of the low-field ^1H NMR spectra of $[(dmpe)MFe_3S_4(LS_3)]^{2-}$ (M = Ni (upper) and Pd (lower)) in CD_3CN solutions at 298 K. Only the 5-H, 6-Me, and 4-Me resonances of LS_3 are shown.

(39) Wei, G.; Liu, H. *Acta Crystallogr.* **1990**, *C46*, 2457−2458.
(40) Landis, K. G.; Hunter, A. D.; Wagner, T. R.; Curtin, L. S.; Filler, F. L.; Jansen-Varnum, S. A. *Inorg. Chim. Acta* **1998**, *282*, 155−162.
(41) Su, W.; Hong, M.; Cao, R.; Liu, H. *Acta Crystallogr.* **1997**, *C53*, 66−67.
(42) Singhal, A.; Jain, V. K.; Varghese, B.; Tiekink, E. R. T. *Inorg. Chim. Acta* **1999**, *285*, 190−196.
(43) Lobana, T. S.; Verma, R.; Hundal, G.; Castineiras, A. *Polyhedron* **2000**, *19*, 899−906.
(44) Briant, C. E.; Calhorda, M. J.; Hor, T. S. A.; Howells, N. D.; Mingos, D. M. P. *J. Chem. Soc., Dalton Trans.* **1983**, 1325−1330.
(45) Bevilacqua, J. M.; Zuleta, J. A.; Eisenberg, R. *Inorg. Chem.* **1994**, *33*, 258−266.
(46) Wei, G.; Huang, Z.; Hong, M.; Liu, H. *Jiegou Huaxue (J. Struct. Chem.)* **1991**, *10*, 159−161.
(47) Mas-Ballesté, R.; Aullón, G.; Champkin, P. A.; Clegg, W.; Mégret, C.; González-Duarte, P.; Lledós, A. *Chem.-Eur. J.* **2003**, *9*, 5023−5035.
(48) Shannon, R. D. *Acta Crystallogr.* **1976**, *A32*, 751−767.

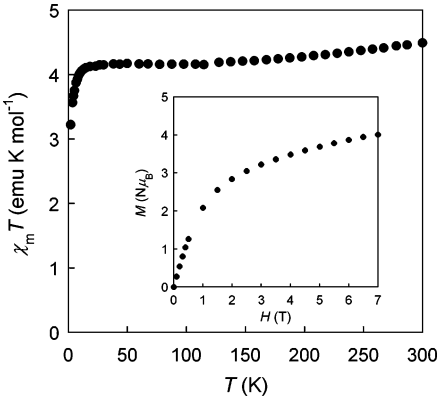

Figure 9. Plot of $\chi_m T$ vs T for polycrystalline $(Et_4N)_2$[(dmpe)$PdFe_3S_4$-(LS_3)] at $H = 1000$ G and $T = 1.8-300$ K. Inset: Plot of magnetization vs H at 2.0 K showing the approach to saturation magnetization.

isotropically shifted resonances in spectra that are readily distinguished from those of $[NiFe_3S_4]^+$ clusters with tetrahedral Ni^{II} sites (Figure 4). Chemical shifts of **13** are δ 16.97, 16.25, and 13.40.

Variable-temperature magnetic susceptibility data for polycrystalline $(Et_4N)_2$[**12**], plotted in Figure 9, were collected to examine the ground state of the cluster. The product $\chi_m T \approx 4.2$ emu K mol^{-1} is nearly constant over the 30−300 K range; $\chi_m T = 4.38$ emu K mol^{-1} for $S = {}^5/_2$.

Magnetic moments calculated from the Curie law at selected temperatures are 5.77 (30 K), 5.83 (180 K), and 5.98 μ_B (300 K). The sharp decrease below 30 K can be ascribed to zero-field splitting effects, while the slightly rising trend at 180 K could arise from the population of levels with high spin multiplicities. Variable-field magnetization data over the 2−4 K range (not shown) reveal nonsuperimposed curves indicative of zero-field splitting. Magnetization data at 2.0 K approach but do not reach saturation while exceeding a value of ~4 N μ_B at 7 T. The collective magnetic data are in accord with an $S = {}^5/_2$ ground state arising from the $[Fe_3S_4]^-$ fragment. This ground state applies to **9**, as deduced from Mössbauer and EPR spectroscopies, whose analysis is complicated owing to structural heterogeneity and lesser stability of clusters.[16] Clusters **9** and **12** are the only synthetic Fe_3S_4 clusters proven to have the $S = {}^5/_2$ ground state. It is highly probable that Pt^{II} cluster **13** has this same ground state. This state has been observed spectroscopically in protein-bound $[ZnFe_3S_4]^+$ clusters.[49−51] The prevailing electronic description invokes an $Fe^{2.5+}Fe^{2.5+}$ valence-delocalized pair and a high-spin Fe^{II} site.[52] Because isotropic shifts in Fe−S clusters are dominantly contact in origin and thus proportional to magnetic susceptibility,[53,54] the difference in ground states is responsible for the larger shifts of **9**, **12**, and **13** vs **2**−**5**.

(c) Structural Relation to *Ch* CODH II C-Cluster. To examine the structural relationship between the native and synthetic clusters, corresponding core fragments were subjected

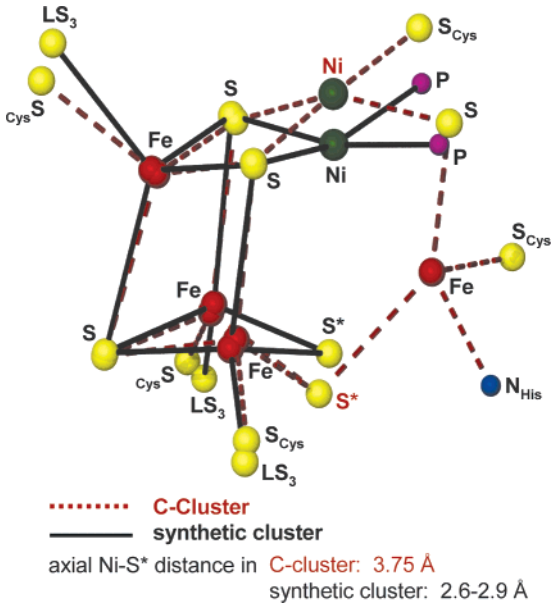

Figure 10. Superposition of the core structures of $[(dmpe)NiFe_3S_4(LS_3)]^{2-}$ (Ni···S* = 2.60 Å) and *Ch* CODH II (1.12 Å resolution).

to best-fit superpositions and weighted rms deviations in atom positions were calculated. The subroutine OFIT of the SHELXL-97 program package was used. The exo iron atom and all bridging and terminal ligand atoms not part of the $NiFe_3S_4$ core were excluded. The situation is illustrated in Figure 10, where a $NiFe_3S_4$ cluster was used with a Ni···S* separation of 2.60 Å.[16] For the Fe_3S_3 portions (excluding S*) the deviation is relatively small (0.088 Å), and it becomes larger for Fe_3S_4 (0.17 Å) and for $NiFe_3S_4$ (0.31 Å). The Fe_3S_3 parts are essentially congruent. The larger rms deviations arise from differences in positions of the Ni and S* atoms. In synthetic clusters, the dihedral angles α and β (Table 2), involving planes containing M and S* atoms, are apparently subject to crystalline effects. In the two crystallographically inequivalent clusters of **12**, $\alpha = 23.0°$ and 31.9° and $\beta = 24.2°$ and 29.4°, resulting in M···S* distances of 3.017(4) and 3.271(4) Å, respectively. Comparable differences in dihedral angles are found with the clusters of **13**, where the distances are 3.107(3) and 3.392(3) Å. On this basis, it would seem plausible that Ni···S* distances are influenced by protein structure and environment.

Site-Differentiated Fe_4S_4 Clusters. In further attempts to construct a planar Ni^{II} site, clusters **2** and **5** were reacted in acetonitrile with potential bidentate chelate ligands containing one thiolate. Reactions were monitored by ^{1}H NMR spectroscopy. When **5** was treated with ca. 1 equiv of the sodium salts of $R_2PCH_2CH_2SH$ (R = Me, Ph), 1,2-$Ph_2PC_6H_4SH$, and Me_2-NCH_2CH_2SH, gradual formation of $[Fe_4S_4]^{2+}$ clusters with ligand bound to the subsite-differentiated iron site was observed (see below). Reactions with **2** led mainly to removal of nickel and formation of cuboidal cluster **1**. In no case was a cluster containing a planar Ni^{II} site detected.

To characterize two of the foregoing reaction products, the reactions of Figure 11 were pursued. The 3:1 site-differentiated cluster **7** reacted smoothly with the specified phosphino- or aminothiolate to afford clusters **15** (76%) and **16** (80%), isolated in the indicated yields as Et_4N^+ salts. In addition, the more soluble compounds $(Bu_4N)_2$[**15**] (82%) and $(Bu_4N)_2$[**16**] (77%) were prepared. The ^{57}Fe isomer shifts $\delta = 0.44-0.45$ mm/s

(49) Surerus, K. K.; Münck, E.; Moura, I.; Moura, J. J. G.; LeGall, J. *J. Am. Chem. Soc.* **1987**, *109*, 3805−3807.
(50) Srivastava, K. K. P.; Surerus, K. K.; Conover, R. C.; Johnson, M. K.; Park, J.-B.; Adams, M. W. W.; Münck, E. *Inorg. Chem.* **1993**, *32*, 927−936.
(51) Finnegan, M. G.; Conover, R. C.; Park, J.-B.; Zhou, Z. H.; Adams, M. W. W.; Johnson, M. K. *Inorg. Chem.* **1995**, *34*, 5358−5369.
(52) Belinsky, M. I. *Chem. Phys.* **2001**, *263*, 279−300.
(53) Reynolds, J. G.; Laskowski, E. J.; Holm, R. H. *J. Am. Chem. Soc.* **1978**, *100*, 5315−5322.
(54) Bertini, I.; Ciurli, S.; Luchinat, C. *Struct. Bonding* **1995**, *83*, 1−53.

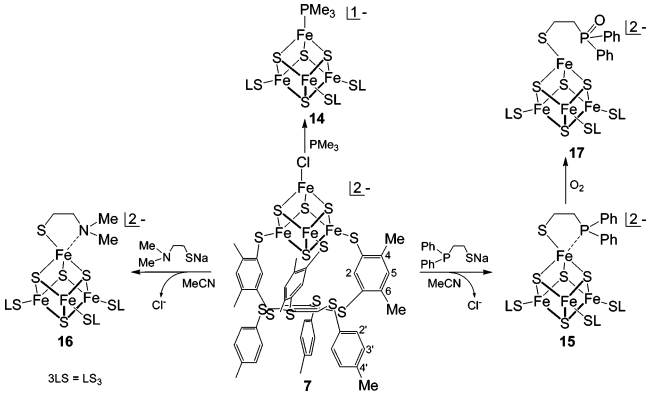

Figure 11. Synthesis of the clusters $[Fe_4S_4(LS_3)(PMe_3)]^{2-}$ (**14**), $[Fe_4S_4(LS_3)(SCH_2CH_2PPh_2)]^{2-}$ (**15**), $[Fe_4S_4(LS_3)(SCH_2CH_2NMe_2)]^{2-}$ (**16**), and $[Fe_4S_4(LS_3)(SCH_2CH_2P(O)Ph_2)]^{2-}$, (**17**).

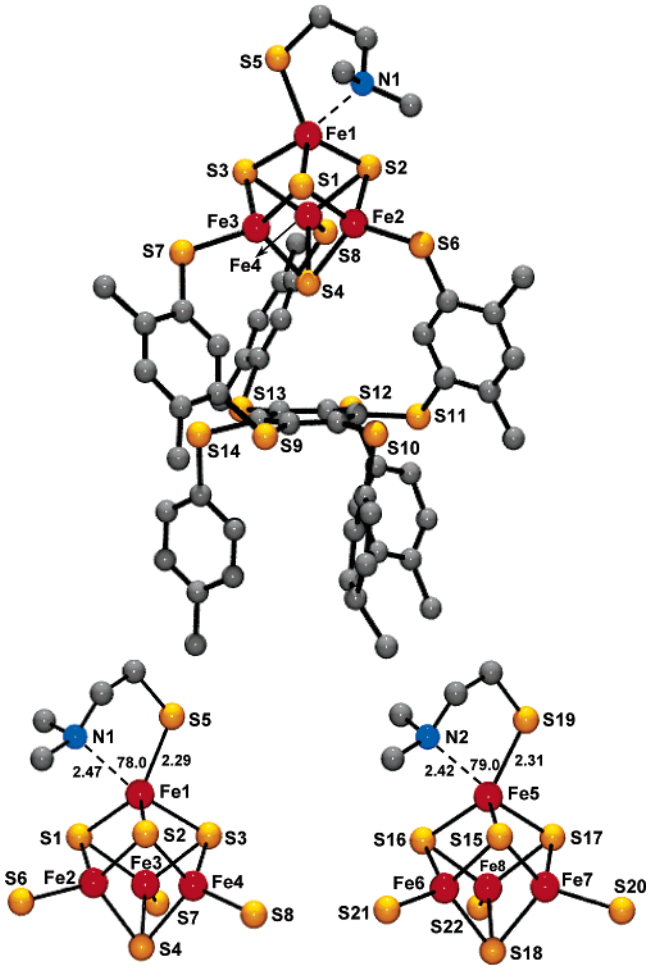

Figure 12. Structure of one of two inequivalent clusters of $[Fe_4S_4(LS_3)(SCH_2CH_2NMe_2)]^{2-}$ (upper), and structures of the Fe_4S_4 portions of both clusters with partial atom labeling schemes and selected bond lengths (Å) and angles (deg) at the unique iron site. Both clusters have the ligand in the *ababab* conformation.

identify the $[Fe_4S_4]^{2+}$ oxidation state,[55] thiolate binding is confirmed by downfield-shifted SCH_2 resonances at 12.05 (**15**) and 20.90 (**16**),[36] and the reduction potentials of −1.11 (**15**) and −1.14 V (**16**) are consistent with alkylthiolate ligation.[22,56] Trimethylphosphine cluster **14** (analogous to **3**) was generated

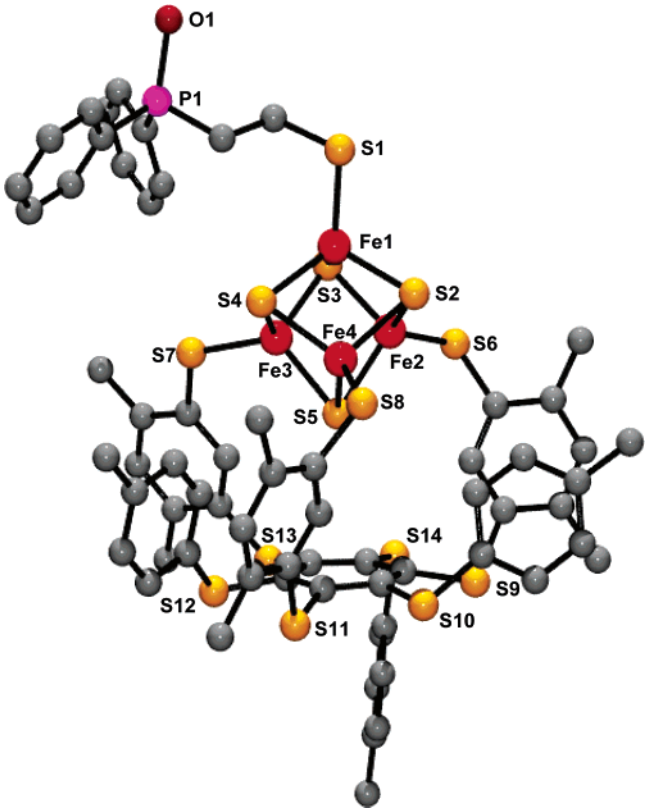

Figure 13. Structure of $[Fe_4S_4(LS_3)(SCH_2CH_2P(O)Ph_2)]^{2-}$ with partial atom labeling scheme; the ligand has the *aaaaab* conformation.

in solution. Its 5-H (8.19) and 4-,6-Me (3.86, 3.83) chemical shifts, compared to those of **15** (8.16, 3.83, 3.71), indicate that LS_3 resonances do not allow assignment of Fe−SR vs Fe−PR_3 binding in this case; the SCH_2 shift is unambiguous in this respect.

The compound $(Et_4N)_2$[**16**] as the acetonitrile solvate crystallizes with two inequivalent clusters in the asymmetric unit. Both have the same overall structure, shown in Figure 12, with the ligand in the *ababab* conformation. The most interesting feature is the coordination at the unique site, depicted for both clusters, where the aminothiolate ligand forms a chelate ring with a normal or perhaps slightly elongated (by ≳0.05 Å) Fe−S bond and a substantially longer Fe−N bond. This is one of the few isolated $[Fe_4S_4]^{2+}$ clusters which have been shown to have five- or six-coordination at the unique site,[18,21−23,57] and the only such cluster with a structurally defined FeS_4N unit. Retention of a chelated structure in solution is apparently the cause of the strongly downfield-shifted SCH_2 signal. Five- or six-coordinate sites in $[Fe_4S_4]^{2+}$ are usually reflected by isomer shifts above ca. 0.50 mm/s at 4.2 K.[21,55] Evidently, Fe−N binding at 2.42−2.47 Å is an insufficient perturbation on the FeS_4 site to influence the Mössbauer parameters. Attempts to obtain diffraction-quality crystals containing **15** were not successful. However, in one such attempt adventitious oxidation led to crystallization of the phosphine oxide cluster **17** as the Et_4N^+ salt acetonitrile hemisolvate. The cluster structure, presented in Figure 13, reveals binding only by thiolate at the unique site and a case of the unusual ligand conformation *aaaaab*. Cluster

(55) Rao, P. V.; Holm, R. H. *Chem. Rev.* **2004**, *104*, 527−559.
(56) DePamphilis, B. V.; Averill, B. A.; Herskovitz, T.; Que, L., Jr.; Holm, R. H. *J. Am. Chem. Soc.* **1974**, *96*, 4159−4167.
(57) Osterloh, F.; Saak, W.; Haase, D.; Pohl, S. *Chem. Commun.* **2000**, 777−778.

Table 4. Selected Interatomic Distances (Å) and Angles (deg) for Site-Differentiated Fe_4S_4 Clusters $[Fe_4S_4(LS_3)(SCH_2CH_2NMe_2)]^{2-}$ (**16**) and $[Fe_4S_4(LS_3)(SCH_2CH_2P(O)Ph_2]^{2-}$ (**17**)

	16[a]		**17**
Fe1−S5/S1[b]	2.294(3)		2.248(1)
Fe1−N1	2.47(1)		
Fe1−S1/S2	2.323(3)		2.255(1)
Fe1−S2/S4	2.278(3)		2.309(1)
Fe1−S3	2.437(3)		2.284(1)
Fe2−S1/S3	2.259(3)		2.276(1)
Fe2−S2	2.311(3)		2.281(1)
Fe2−S4/S5	2.299(3)		2.303(1)
Fe3−S1/S5	2.293(3)		2.273(1)
Fe3−S3	2.274(3)		2.315(1)
Fe3−S4	2.254(3)		2.277(1)
Fe4−S2	2.294(3)		2.297(1)
Fe4−S3/S4	2.249(3)		2.267(1)
Fe4−S4/S5	2.295(3)		2.281(1)
Fe−SL[c]	2.279(1)		2.257(6)
S4/S5−ctr[d]	3.673(5)		3.736(2)
S1−Fe1−S5	128.4(1)	S2−Fe1−S1	108.90(5)
S2−Fe1−S5	123.8(1)	S3−Fe1−S1	117.41(4)
S3−Fe1−S5	90.9(1)	S4−Fe1−S1	116.24(5)
S2−Fe1−S3	97.5(1)	S4−Fe1−S2	104.72(2)
S3−Fe1−N1	168.5(3)		
S1−Fe1−S2	105.4(1)		
S1−Fe1−S3	98.2(1)		

[a] Et_4N^+ salt; one of two inequivalent clusters. [b] Atom labels in order **16**/**17**. [c] Mean value of terminal bond lengths. [d] Distance from S4/S5 to the centroid of the central benzene ring.

dimensions of **16** and **17**, summarized in Table 4, are unexceptional.[37]

Summary. The following are the principal results and conclusions of this investigation, together with certain results from previous work.

(1) Cubane-type $[NiFe_3S_4]^+$ clusters containing *tetrahedral* Ni^{II} sites can be formed by two procedures: (i) metal ion incorporation into cuboidal $[Fe_3S_4(LS_3)]^{3-}$ by reaction with Ni^0, Ni^I,[17] or Ni^{II}/RS^- species, and (ii) reaction of Ni^0 species with linear $[Fe_3S_4(SR)_4]^{3-}$.[14,15] Product clusters are of the general type $[LNiFe_3S_4(SR)_3]^{2-}$ (L = R_3P, RNC). The procedures are examples of cluster formation by fragment condensation, with (ii) including the subsequent step of core rearrangement.[58]

(2) The clusters described in (1) undergo a limited set of substitution reactions at the Ni^{II} site, including displacement of Ph_3P by Bu^tNC, R_3P, and RS^-,[14] displacement of Bu^tNC by R_3P (R = alkyl), and metal removal by chelating dithiolates to give the cuboidal $[Fe_3S_4]^0$ cluster.

(3) Cubanoid $[NiFe_3S_4]^+$ clusters containing *planar* Ni^{II} sites are accessible by two procedures: (i) displacement of Ph_3P with the chelating diphosphines $R_2PCH_2CH_2PR_2$ (R = Me,[16] Et, Ph), and (ii) metal atom incorporation into $[Fe_3S_4(LS_3)]^{3-}$ using a Ni^0 reactant in the presence of $Me_2PCH_2CH_2PMe_2$. Procedure (ii) with Pd^0 and Pt^0 affords the analogous clusters $[(dmpe)M^{II}Fe_3S_4(LS_3)]^{2-}$.

(4) The most conspicuous structural features of the product clusters described in (3) are planar diamagnetic MP_2S_2 coordination units with variable separations of the metal ion from an axial μ_2-S atom: M···S* = 2.60−2.90 Å (Ni);[16] 3.02, 3.27 Å (Pd); 3.11, 3.39 Å (Pt). Reaction (i) described in (3) results in a tetrahedral/planar structural change with retention of core atoms. Planar stereochemistry is stabilized by a strong in-plane ligand field at Ni^{II} and is the dominant structural preference for Pd^{II} and Pt^{II}.

(5) The $[NiFe_3S_4]^+$ oxidation level with tetrahedral Ni^{II} has an $S = {}^3/_2$ ground state arising from antiferromagnetic coupling of $S = 1$ (Ni^{2+}) and $S = {}^5/_2$ ($[Fe_3S_4]^-$),[15,50,59] while $[NiFe_3S_4]^+$ with planar Ni^{II} has an $S = {}^5/_2$ ground state, previously observed in protein-bound $[ZnFe_3S_4]^+$ clusters. This statement is supported by the magnetism of $[(dmpe)PdFe_3S_4(LS_3)]^{2-}$. Consequently, the two structural isomers of the $[NiFe_3S_4]^+$ core are conveniently distinguished by their isotropically shifted ^1H NMR spectra.

This work and that preceding it[16] demonstrate that a planar M^{II} site can be stabilized within the $[MFe_3S_4]^+$ cubanoid core. A planar Ni^{II} site is a structural element of at least the C-cluster of *Ch* CODH II (Figure 1). Hence, the feasibility of step (i) in the synthesis of the C-cluster structure is demonstrated. To proceed further, it will be necessary to incorporate bridging atoms, perhaps in physiologically credible bidentate ligands, that promote binding of the exo iron atom to form the full $NiFe_4S_5$ core. Clusters **9**, **12**, and **13** first offer the possibility of examining the metal binding affinity of the S* atom positioned at 2.6−3.4 Å from the heterometal site.

Acknowledgment. This research was supported by NIH Grant GM 28856. We thank Professor K. R. Dunbar for generous access to the magnetometer and Dr. S. C. Lee for useful discussions.

Supporting Information Available: X-ray crystallographic files for the five compounds in Table 1 (CIF). This material is available free of charge via the Internet at http://pubs.acs.org.

JA052381S

(58) Lee, S. C.; Holm, R. H. *Chem. Rev.* **2004**, *104*, 1135−1157.

(59) Johnson, M. K.; Duderstadt, R. E.; Duin, E. C. *Adv. Inorg. Chem.* **1999**, *47*, 1−82.